NANO LETTERS

Letter

pubs.acs.org/NanoLett

A Yolk-Shell Design for Stabilized and Scalable Li-Ion Battery Alloy Anodes

Nian Liu,[†,⊥] Hui Wu,[‡,⊥] Matthew T. McDowell,[‡] Yan Yao,[‡] Chongmin Wang,[§] and Yi Cui*[,‡,∥]

[†]Department of Chemistry and [‡]Department of Materials Science and Engineering, Stanford University, Stanford, California 94305, United States

[§]Environmental Molecular Sciences Laboratory, Pacific Northwest National Laboratory, Richland, Washington 99352, United States

[∥]Stanford Institute for Materials and Energy Sciences, SLAC National Accelerator Laboratory, 2575 Sand Hill Road, Menlo Park, California 94025, United States

Supporting Information

ABSTRACT: Silicon is regarded as one of the most promising anode materials for next generation lithium-ion batteries. For use in practical applications, a Si electrode must have high capacity, long cycle life, high efficiency, and the fabrication must be industrially scalable. Here, we design and fabricate a yolk-shell structure to meet all these needs. The fabrication is carried out without special equipment and mostly at room temperature. Commercially available Si nanoparticles are completely sealed inside conformal, thin, self-supporting carbon shells, with rationally designed void space in between the particles and the shell. The well-defined void space allows the Si particles to expand freely without breaking the outer carbon shell, therefore stabilizing the solid-electrolyte interphase on the shell surface. High capacity (~2800 mAh/g at C/10), long cycle life (1000 cycles with 74% capacity retention), and high Coulombic efficiency (99.84%) have been realized in this yolk-shell structured Si electrode.

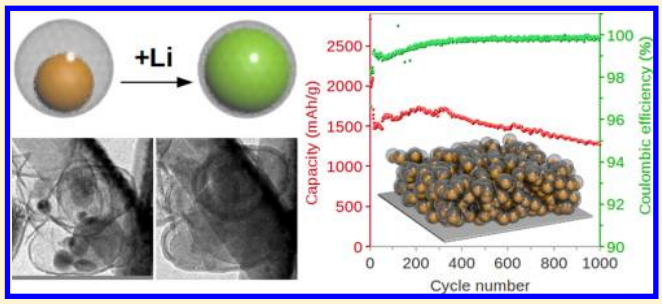

KEYWORDS: *Silicon nanoparticle, Li-ion battery, anode, yolk-shell, solid-electrolyte interphase, in situ TEM*

Electrochemical energy storage has become a critical technology for a variety of applications, including grid storage, electric vehicles, and portable electronic devices. The lithium-ion battery (LIB) is an attractive energy storage device because of its relatively high energy density and good rate capability. To further increase the energy density for more demanding applications, however, new electrode materials with higher specific and volumetric capacity are required. Since the initial commercialization of the LIB two decades ago, there has been little progress in commercializing new electrode materials with significantly higher capacity.[1] To meet the increasing demand for energy storage capability, novel electrode materials with higher capacity, low cost, and the ability to be produced at large scale are of great interest.

Alloy-type anodes (Si, Ge, Sn, Al, Sb, etc.) have much higher Li storage capacity than the intercalation-type graphite anode that is currently used in Li-ion batteries.[2] Among all the alloy anodes, silicon has the highest specific capacity: Experiments have demonstrated an initial specific capacity of >3500 mAh/g, which is 10 times the capacity of graphite.[3] In addition, silicon is the second most abundant element in the earth's crust (28% by mass), indicating its potential to be utilized in large quantities at low cost.[4] A further benefit is that mass production of elemental silicon is already a mature technology in the semiconductor industry. Despite these advantages, graphite anodes still dominate the marketplace due to the fact that alloy anodes have two major challenges that have prevented their widespread use. First, alloy anodes undergo significant volume expansion and contraction during Li insertion/extraction.[2] This volume change (~300% for Si) can result in pulverization of the initial particle morphology and causes the loss of electrical contact between active materials and the electrode framework. Second, due to the low electrochemical potential of Li insertion/extraction (<0.5 V vs Li^+/Li), the anode surface becomes covered by a solid-electrolyte interphase (SEI) film, which forms due to the reductive decomposition of the organic electrolyte.[5] In graphite anodes, a thin passivating SEI forms during the first few cycles, and its further formation is terminated due to the electronically insulating nature of the SEI.[6] In alloy anodes, however, the SEI will rupture due to the volume change during cycling, causing the electrode surface to be cyclically exposed to the electrolyte. This results in continual formation of very thick SEI films, which causes the electrolyte to be continually consumed during cycling. The formation of SEI is further complicated by particle fracture, since fracture creates new active surfaces for SEI growth. The excessive growth of SEI causes low Coulombic efficiency, higher resistance to ionic transport, and low electronic conductivity

Received: April 20, 2012

 © XXXX American Chemical Society

of the whole electrode, and it will eventually result in the exhaustion of the electrolyte and dry-out of the cell.[7]

Recent work has shown that reducing the size of bulk silicon to the submicrometer scale in at least one dimension can effectively avoid fracture and therefore improve the cycling performance.[3,8−12] Most of these nanostructures are fabricated by chemical vapor deposition (CVD) from a silane gas precursor, which is expensive and difficult to scale up. Silicon nanoparticles (SiNPs), on the other hand, are a promising candidate because they are commercially available, industrially scalable, and compatible with the current slurry coating manufacturing process for LIB electrodes. However, conventional polyvinylidene fluoride (PVDF) binder does not connect the SiNPs well because of the dramatic volume changes and displacement of particles during cycling. To overcome this problem, several novel binders have been reported, such as sodium alginate, poly(acrylic acid) (PAA), sodium carboxymethyl cellulose (CMC), and conductive binder.[13−16] Even though these binders result in well-connected electrodes and minimal loss of active materials, the surfaces of silicon particles are still directly exposed to the electrolyte and unstable SEI formation remains a problem.

To tackle this problem, conformal coatings on Si anode structures have been explored.[17,18] Though the low working potential of the anode limits the choice of coating materials, some coatings, including amorphous carbon and metallic coatings, have shown good chemical stability. However, upon the volume expansion of Si, these coatings will fracture, and the Si surface will still be exposed to electrolyte.[19]

Very recently, Si nanotubes confined in SiO_x outer shells (termed the double-walled Si-SiO_x nanotube anode) have demonstrated excellent electrochemical performance.[20] The void space in the center and the outer SiO_x clamping layer force the Si tube to expand inward during lithiation. Therefore, the SEI formed on the outer surface of the SiO_x shell remains intact during cycling and does not continually grow, resulting in thin SEI films and stable cycling for thousands of cycles. Even though the fabrication process still utilizes silane CVD, this structure proves that this is an effective way to control the SEI growth on Si anodes. In addition, SiNPs embedded in tubular carbon structures have been demonstrated.[21,22] The empty space around the SiNPs allows the SiNPs to expand without rupturing the carbon tubes. Therefore, a thin and stable SEI on the surfaces of the carbon tubes is maintained, which results in stable cycling for over 200 cycles. Unfortunately, long tubes are needed to prevent electrolyte ingress into the two ends, which makes this initial demonstration not fully compatible with current slurry coating manufacturing process. Also, the distribution of the SiNPs inside the carbon tubes is not well-defined.

Intentionally controlling the size and distribution of porosity inside the SiNP-based electrodes to allow for volume expansion/contraction has been a challenge. The slurry drying process generates pores inside the electrode, but they are randomly distributed and randomly sized (Figure 1A). In other words, even though the total empty space is enough for the Si volume expansion, the local porosity around each individual particle might not be sufficient to accommodate volume expansion. Therefore, a successful design must take into account all of the above considerations: nanostructuring of Si, formation of a stable SEI, well-controlled pore space, and scalable fabrication.

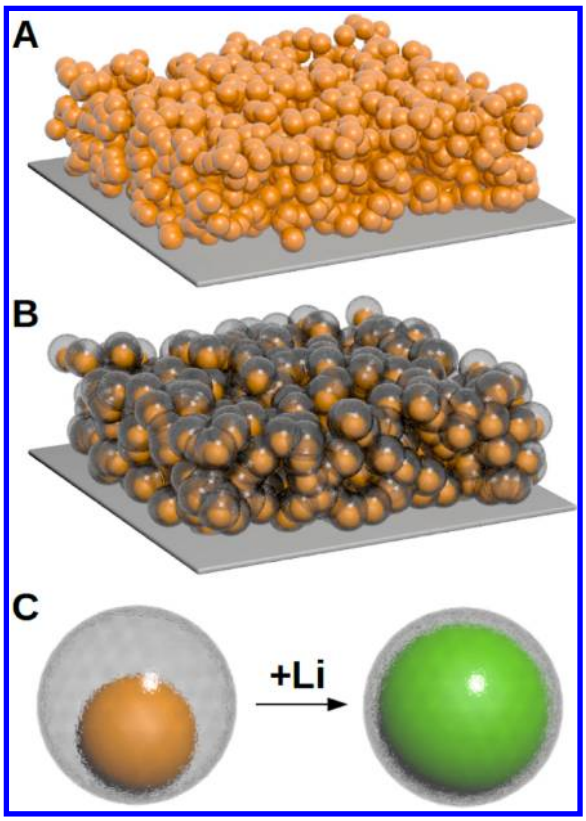

Figure 1. Schematic of the materials design. (A) A conventional slurry coated SiNP electrode. SEI on the surface of the SiNPs ruptures and reforms upon each SiNP during cycling, which causes the excessive growth of SEI and failure of the battery. The expansion of each SiNP also disrupts the microstructure of the electrode. (B) A novel Si@void@C electrode. The void space between each SiNP and the carbon coating layer allows the Si to expand without rupturing the coating layer, which ensures that a stable and thin SEI layer forms on the outer surface of the carbon. Also, the volume change of the SiNPs is accommodated in the void space and does not change the microstructure of the electrode. (C) A magnified schematic of an individual Si@void@C particle showing that the SiNP expands without breaking the carbon coating or disrupting the SEI layer on the outer surface.

Here, we design a "yolk-shell" structure for a stabilized and scalable Si anode. The structure has SiNPs (∼100 nm) as the "yolk" and amorphous carbon (5−10 nm thick) as the "shell" (Figure 1B). Each SiNP is attached to one side of the carbon shell, while there is an 80−100 nm void space on the other side. This yolk-shell structure has several advantages for LIB alloy anodes. First, the carbon shell is a self-supporting framework, and the well-controlled void space between the SiNPs and the carbon shell allows for the SiNPs to expand upon lithiation without breaking the carbon (Figure 1C). This in turn allows for the growth of a stable SEI on the static surface of the carbon shell and prevents the continual rupturing and reformation of the SEI. Second, the carbon shell is uniform and mostly free of pinholes, which prevents the electrolyte from reaching the SiNP surface inside the shell. Lithiation of the Si occurs by Li diffusion through the carbon shell into the Si core. Even if there are some minor imperfections or pinholes in the carbon shell initially, the SEI formed on the carbon shell will fill the holes and isolate the inside of the shell from the electrolyte with cycling. Third, the carbon shell is both electronically and ionically conducting, which allows for good kinetics. Fourth,

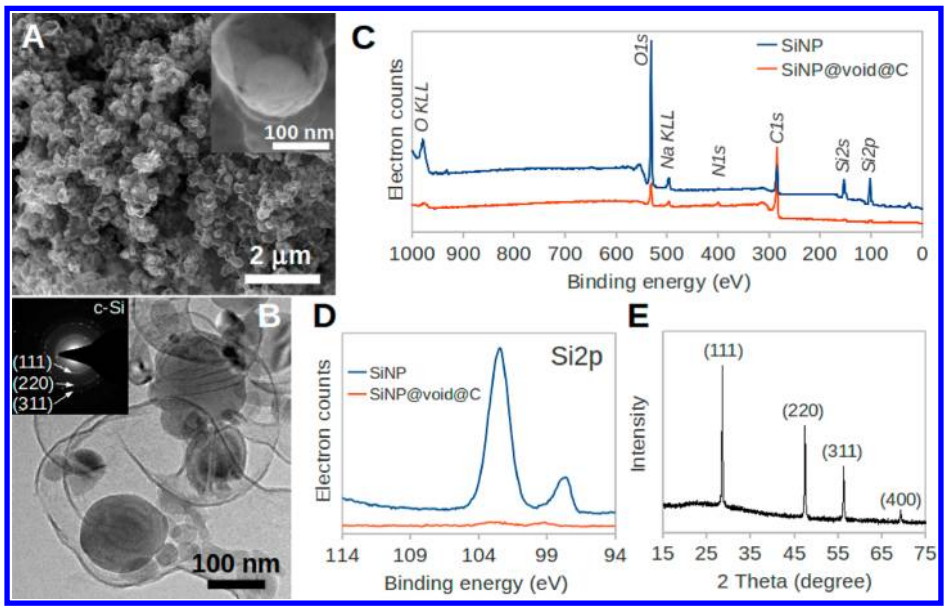

Figure 2. Characterization of Si@void@C material and electrodes. (A) SEM and (B) TEM images of synthesized Si@void@C powder. The inset of (A) is a magnified SEM image of one yolk-shell particle. The inset of (B) is the SAED pattern with the diffraction rings indexed. (C) XPS spectra of the electrode surface with active materials consisting of SiNPs and Si@void@C, respectively. Both electrodes were made under the same conditions with carbon additive and alginate binder. (D) High-resolution XPS spectra of the Si2p peaks for the same electrodes. The Si signal is significantly reduced in the Si@void@C electrode. In (C) and (D), both XPS spectra were collected under the same conditions without further processing. (E) XRD pattern of Si@void@C powder. The peaks are all from crystalline Si.

unlike high-aspect-ratio nanotubes or nanowires, the yolk-shell nanostructure is fully compatible with current slurry coating technology. Fifth, unlike traditional slurry coated electrodes, our Si@void@C electrode has a well-defined void space around every Si particle, which allows for each particle to expand upon lithiation without deforming the electrode microstructure.

We have developed a room temperature solution method to conformally coat SiNPs first with a SiO_2 sacrificial layer and then with a polydopamine layer, which is subsequently carbonized to form a nitrogen-doped carbon coating. After selectively removing the SiO_2 sacrificial layer by hydrofluoric acid (HF) treatment, the yolk-shell Si@void@C structure is obtained (Figure 2A,B). The whole fabrication is scalable, and the powder-like product is fully compatible with current slurry coating technology (Figure S1, Supporting Information). The solution coating method was chosen instead of a solid or gas phase method because it produces a conformal, homogeneous coating on every individual particle (Figure S2, Supporting Information). The homogeneity of the coating is crucial to a successful yolk-shell design because ideally the shell should prevent electrolyte ingress so the SEI is formed only on the outside of the shell. While we were preparing this manuscript, a paper was published in which a similar structure was studied, but a gas-phase carbon coating method was used, which results in a nonconformal coating. Uncoated (bare) Si surface is evident from the X-ray photoelectron spectroscopy (XPS) analysis, in which the Si2p signal is still strong in the coated sample.[23] In addition, the cycling performance of the coated Si is not much different than that of bare SiNPs. Therefore, a conformal and homogeneous coating is crucial for good electrochemical performance of the yolk-shell structure.

We have used a sol–gel method to conformally coat amorphous SiO_2 onto the SiNPs. Because the SiNPs have native oxide on the surface, the decomposition of tetraethyl orthosilicate (TEOS) in ammonia solution occurs preferentially on the SiNP surfaces.[24] By controlling the TEOS concentration, pH, and coating time, the thickness of the SiO_2 coating and therefore the void space size can be easily controlled (Figure S3, Supporting Information).[25,26] The SiNPs utilized for this study have an average diameter around 100 nm. Smaller particles might yield better battery performance, but they are more costly as well. Therefore we have chosen the commercially available ~100 nm particles. Assuming a 300–400% volume expansion of crystalline Si upon complete lithiation,[27] the sacrificial coating thickness should be >30 nm to allow an individual SiNP to expand without rupturing the shell. Taking into account the size variation of the SiNPs, we control the thickness of the SiO_2 layer to be about 40–50 nm in further experiments.

The second coating of polydopamine was conducted by the self-polymerization of dopamine in a solution of pH 8.5 in the presence of oxygen. This coating method has been reported to give a highly conformal polydopamine coating with a thickness that can be controlled by varying the coating time.[28] The silica sol is stable in a pH window between 8 and 11, so the SiO_2 layer is stable during the polydopamine coating process.[29] The carbon precursor has an important effect on the morphology and properties of the resulting carbon coating. Polydopamine has been reported to yield highly conformal and effective carbon coatings.[30] The carbon coating obtained here is 5–10 nm in thickness (see the TEM image in Figure 2B). Its presence is also evident from the enhanced XPS C1s peak (Figure 2C), and it is mostly amorphous according to selected-area electron diffraction (SAED) (Figure 2B, inset) and X-ray diffraction (XRD) results (Figure 2E). Moreover, XPS results show that the carbon layer is nitrogen-doped (Figure 2C); the nitrogen originates from the dopamine precursor, and it comprises 2.2% of the elements on the electrode surface. This probably benefits the electrochemical performance, since nitrogen doping has been reported to facilitate the electronic

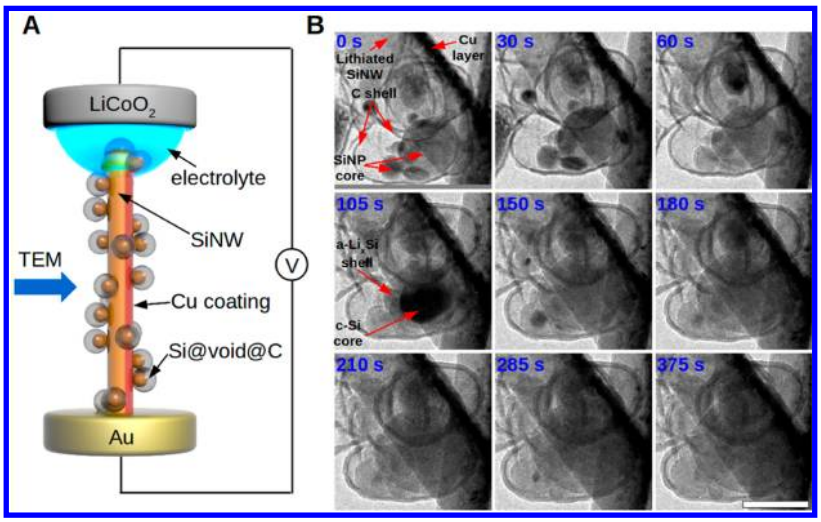

Figure 3. In situ TEM characterization of Si@void@C expansion during electrochemical lithiation. (A) Schematic of the in situ TEM device. (B) In situ TEM image series captured from movie S1, Supporting Information. In this series of images, the silicon particles are observed to expand within the outer carbon shell. The entire volume expansion is accommodated within the available void space, and the shell does not rupture. In addition, these data indicate that Li transport through the carbon layer is sufficient for good rate capability. Scale bar: 200 nm.

conductivity of the carbon layer and the charge transfer at the interface.[31] The rigidity of the thin carbon coating allows it to form a self-supporting shell outside the SiNP core (Figure 2A,B) after the removal of the SiO_2 sacrificial layer. Some carbon shells contain more than one SiNP, which is due to slight aggregation during SiO_2 coating or polydopamine coating. It is important to note that most individual SiNPs contact the outer shell in at least one location in the final product, which allows for Li transport from the carbon shell into the SiNPs during lithiation. All these fabrication steps are carried out at room temperature except for carbonization. No silane precursor is used, and the whole process is easily scalable.

As discussed, the key of the yolk-shell design is the self-supporting and conformal shell that separates the SiNPs from the electrolyte. To determine if our synthesized Si@void@C material has a high-quality yolk-shell structure, we conducted surface sensitive high-resolution XPS on Si2p peaks for SiNP and Si@void@C electrodes (Figure 2D). The Si@void@C electrode shows a negligible Si signal compared to the SiNP electrode. The XPS elemental analysis shows that the surface atomic percentage of Si decreases from 15.9% in the bare SiNP electrode to 1.4% in Si@void@C electrode, while the percentage of carbon increases from 32.3% to 85.6%. Therefore, in our synthesized Si@void@C material, the SiNPs appear to be completely sealed inside the hollow carbon shell, though there might be some nanoscale pores in the carbon walls since HF can diffuse into the structure to etch away the SiO_2. We hypothesize that this nearly completely sealed structure is crucial for obtaining excellent electrochemical cycling performance. The nanoscale pores will be blocked by the SEI formation after initial battery cycling, which will prevent the direct contact of SiNPs with the electrolyte.

The recent application of in situ TEM to study electrochemical reactions has provided a powerful way to monitor the structural changes of materials during electrochemical processes.[32,33] Here, we use this in situ TEM technique to observe the deformation and structural changes during lithiation of the Si@void@C material to gain insight into the volume change process. The in situ electrochemical cell is shown schematically in Figure 3A. Si@void@C particles are first drop-cast onto Si nanowires (NWs) grown on a flat Si substrate. The NWs have a thin layer of copper thermally evaporated onto their surface to improve electrical conductivity in the device.[19] A few NWs with the attached Si@void@C particles are then transferred to a metallic probe on a specialized dual-probe biasing TEM holder, as shown at the bottom of the schematic. $LiCoO_2$ particles are attached to the other metallic probe (the top of the schematic), and a drop of ionic liquid electrolyte is placed on this electrode. The ionic liquid has extremely low vapor pressure and therefore does not evaporate when exposed to the high vacuum of the TEM column. Inside the TEM, the NW is positioned so that the NW tip is immersed in the ionic liquid. In this way, a nanoscale electrochemical device is formed where the NW/Si@void@C electrode is the working electrode and the $LiCoO_2$ is the Li-containing counter electrode. By applying a −4 V bias to the NW side, Li^+ is reduced and diffuses into the NW. Since the Si@void@C particles are physically attached to the NW, the particles also become lithiated due to Li diffusion between the structures. While this experimental geometry is obviously different than in an actual battery, the deformation characteristics are expected to be similar, especially since fast surface diffusion causes lithiation to proceed relatively uniformly in the Si particles.[9]

Figure 3B shows a series of images taken from a movie of the in situ lithiation of Si@void@C particles (movie S1, Supporting Information). In the first image (0 s), pristine Si nanoparticles are visible within the surrounding C shell. The already fully lithiated NW that is in physical contact with the Si@void@C particles is also seen in the frame (the NW has the $Li_{15}Si_4$ structure). In subsequent frames, the Si particles expand in volume as Li diffuses through the carbon coating and reacts with the Si particles. The volume expansion is most evident in the set of particles at the bottom of the structure. In the frame labeled "105 s", the particles are partially lithiated, and an amorphous Li_xSi shell/crystalline Si core structure is readily discernible in the largest particle (the crystalline core is the region with dark contrast). This two-phase reaction mechanism is well-known to occur during the lithiation of crystalline Si.[34] After complete lithiation, the diameter of the largest particle increases from ∼185 to ∼300 nm. Fracture was not observed in

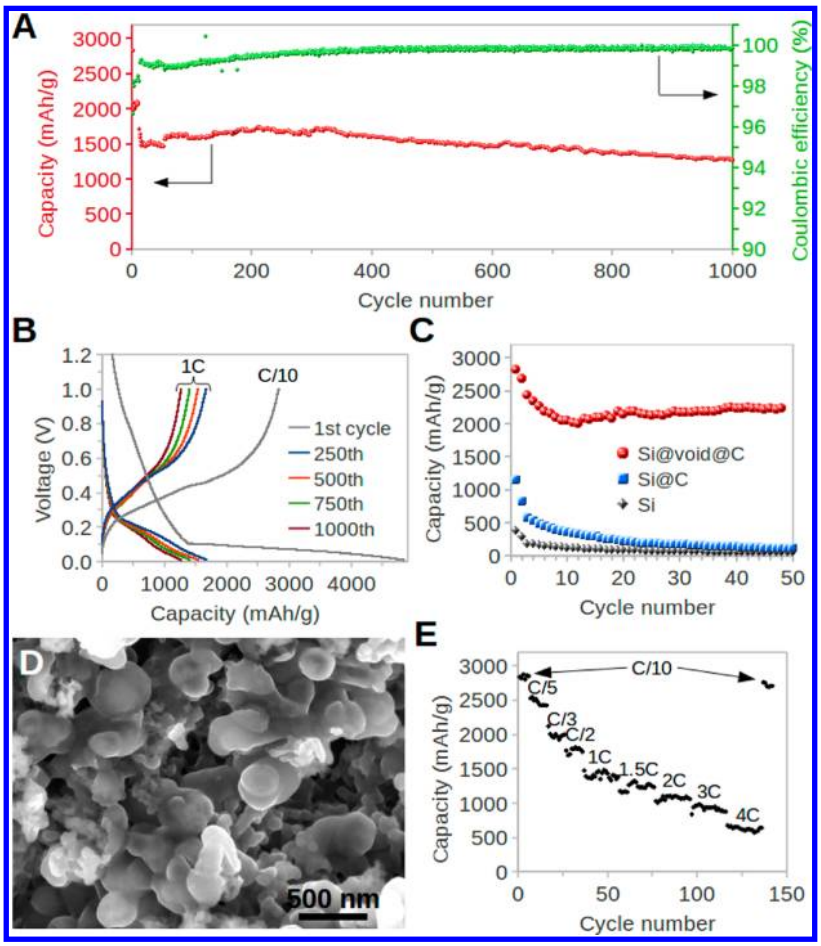

Figure 4. Electrochemical cycling results for Si@void@C electrodes. (A) Delithiation capacity and CE of the first 1000 galvanostatic cycles between 0.01−1 V (alginate binder). The rate was C/10 for one cycle, then C/3 for 10 cycles, and 1C for the later cycles. (B) Voltage profiles plotted for the first, 250th, 500th, 750th, and 1000th cycles. (C) Galvanostatic cycling of different silicon nanostructures (PVDF binder). All samples were cycled at C/50 for the first cycle, C/20 for the second cycle, and C/10 for the later cycles. (D) SEM image of Si@void@C electrode after 800 electrochemical cycles, showing the Si−C yolk-shell structure coated with a uniform thin SEI layer. (E) Delithiation capacity of Si@void@C with alginate binder cycled at various rates from C/10 to 4C.

these particles. In addition, the carbon coating also becomes lithiated; the thickness of the carbon increases from 5 to 10 to ∼20 nm after lithiation without noticeably increasing the size of the shell. Some of the observed increase in the thickness of the carbon shell could also be due to build-up of a thin layer of ionic liquid electrolyte at the surface.

This in situ TEM experiment reveals important details related to the volume changes in this structure. First, in this configuration, Li must diffuse from the lithiated NW through the carbon shell into the individual particles for them to become lithiated. All the Si particles in the observation window were lithiated (Figure 3B and Movie S1 in the Supporting Information). The successful lithiation of the Si particles indicates good contact between the carbon shell and Si particles. In addition, the rate of Li diffusion through the carbon shell (5−10 nm) seems to be fast enough for lithiation to occur in a reasonable time (in this experiment the particles are fully lithiated in ∼340 s). This indicates that even though the silicon and carbon only contact at a small area, reasonable current densities could be supported. Second, it is clear that the carbon coating remains intact after Si expansion even though the expansion causes the Si particles to impinge upon the carbon coating. This could be attributed to (i) the plastic flow of lithiated Si so that it expands into the void space away from the carbon shell[35] and (ii) to the fact that there is enough void space to accommodate the full expansion of each Si particle. Because the overall shape of the yolk-shell structure does not change appreciably upon lithiation, it is expected that a battery electrode made of this Si@void@C structure will undergo minimal microstructural damage upon cycling, in contrast to an electrode made of bare SiNPs. Finally, the void space is carefully designed so that the Si particles occupy almost all the void space after full lithiation, which maximizes the volumetric energy density.

The successful design and fabrication of the yolk-shell structure for a stabilized anode is evident from the excellent electrochemical behavior (Figure 4). The specific capacity values reported are calculated on the basis of the total weight of the Si@void@C material, in which silicon comprises ∼71% of the mass determined by thermogravimetric analysis (TGA, Figure S4, Supporting Information). It should be noted that the carbon shell is also lithiated, as observed in the in situ TEM experiments (Figure 3B). Therefore, both the Si particles and the carbon shell contribute to the capacity. Upon deep galvanostatic cycling between 0.01 and 1 V, the reversible capacity reaches 2833 mAh/g for the first cycle at C/10 and stabilizes at ∼1500 mAh/g for later cycles at 1C (Figure 4A). The specific capacity of our yolk-shell structure is much higher

than other reported carbon coated SiNP structures[23,36] because our specially designed conformal carbon shell, which is 5−10 nm thick, only comprises <30% of the total weight of the Si@void@C material. In addition, the Si@void@C material has a long cycle life (Figure 4A). No capacity decay was observed in the first 300 cycles, and the capacity retention values after 500, 750, and 1000 cycles are 88%, 81%, and 74%, respectively. The voltage profiles for the different cycles are shown in Figure 4B. The shape of the profile does not change from the 250th to the 1000th cycle, indicating stable electrochemical behavior of Si@void@C. Cyclic voltammetry and electrochemical impedance measurements (Figure S5, Supporting Information) also support the presence of highly reversible lithiation/delithiation. Finally, constant capacity galvanostatic cycling with the lithiation capacity limited to 1000 mAh/g results in stable cycling for 1400 cycles (Figure S6, Supporting Information). This excellent cycling stability is attributed to the successful design and synthesis of yolk-shell structure, which allows the individual SiNPs to expand and contract inside the carbon shell without rupturing the SEI built outside the shell or deforming the outer shape of the structure.

To determine any effect of the binder on electrochemical performance, we also tested the cycling performance of the yolk-shell structure with a conventional PVDF binder (Figure 4C); this binder has been reported to result in poor electrochemical performance for alloy-type anodes.[16] At the rate of C/50, the Si@void@C cell shows reversible capacity of 2820 mAh/g, similar to the cell with alginate binder. In contrast, the bare SiNP cell and Si@C cell (SiNPs directly coated with carbon without the void space in between) have specific capacity of only 382 and 1156 mAh/g, respectively. Bare SiNPs have a native oxide on the surface, which not only lowers the specific capacity but also could slow down or limit lithiation in SiNPs.[37,38] The Si@void@C cell has high initial capacity because the native oxide is removed in the final etching step, and the tailored void space allows the Si particles to expand freely with the conductive carbon shell supplying the Li from outside the structure. Moreover, the capacity retention of Si@void@C is much better than bare Si and Si@C particles. The good cycling capability with both alginate and PVDF binder indicates that our design and synthesis of the yolk-shell structure is successful and is an effective anode framework for SiNP-based anodes.

Coulombic efficiency is indicative of the stability of the SEI because rupturing and reforming the SEI will consume Li. The average CE for the Si@void@C cell with alginate binder, from the 500th to the 1000th cycles, is as high as 99.84%, owing to the stable, thin, and smooth SEI built on the outside of the carbon shell. The spherical shapes of the particles are still well resolved after 800 cycles, as shown in the SEM image in Figure 4D. In contrast, the bare SiNP electrode after cycling was coated with a thick and interconnected SEI (Figure S7, Supporting Information). Electrochemical impedance spectroscopy (EIS) results also suggest a stable SEI by showing stable charge-transfer resistance over many cycles (Figure S5B,C, Supporting Information). The stable and thin SEI on the Si@void@C material also enables good rate capability (Figure 4E and Figure S8, Supporting Information). Even at a rate of 4C, the Si@void@C electrode can still achieve a capacity of 630 mAh/g, almost two times that of the theoretical capacity of graphite. The first cycle CE is ∼60% because the initial SEI formation on the carbon surface consumes some lithium, but this drawback could be avoided by performing prelithiation.[39]

In summary, we have designed and fabricated a "yolk-shell" structure for a scalable, electrochemically stable, and highly efficient Si electrode. The fabrication is carried out mostly at room temperature without the use of CVD. The yolk-shell consists of Si particles completely protected by a thin, conformal, and self-supporting carbon shell. Rationally designed void space in between the shell and the particles allows for the expansion of Si without deforming the carbon shell or disrupting the SEI on the outside surface. This structure shows excellent capacity (2833 mAh/g at C/10), cycle life (1000 cycles with 74% capacity retention), and Coulombic efficiency (99.84%). Moreover, the yolk-shell structure still performs well even with conventional PVDF binder, confirming the successful materials design and fabrication. In addition to Si, this yolk-shell structure can also be applied to other high capacity alloy-type anode materials for next generation Li-ion batteries to improve cycle life and Coulombic efficiency.

■ ASSOCIATED CONTENT

Ⓢ Supporting Information

Experimental procedures, optical images, additional SEM images, TGA data, electrochemical characterization, additional voltage profiles, and additional cycling performance. This material is available free of charge via the Internet at http://pubs.acs.org.

■ AUTHOR INFORMATION

Corresponding Author

*E-mail: yicui@stanford.edu

Author Contributions

⊥These authors contributed equally.

Notes

The authors declare no competing financial interest.

■ ACKNOWLEDGMENTS

This work was partially supported by the Assistant Secretary for Energy Efficiency and Renewable Energy, Office of Vehicle Technologies of the U.S. Department of Energy (contract no. DE-AC02-05CH11231) and the Batteries for Advanced Transportation Technologies (BATT) Program (subcontract no. 6951379). M.T.M. acknowledges support from the Chevron Stanford Graduate Fellowship, the National Defense Science and Engineering Graduate Fellowship, and the National Science Foundation Graduate Fellowship. C.M.W. acknowledges support from the Laboratory Directed Research and Development (LDRD) program of Pacific Northwest National Laboratory. The in situ TEM work was conducted in the William R. Wiley Environmental Molecular Sciences Laboratory (EMSL), a national scientific user facility sponsored by DOE's Office of Biological and Environmental Research and located at PNNL. PNNL is operated by Battelle for the DOE under contract DE-AC05-76RLO1830.

■ REFERENCES

(1) Armand, M.; Tarascon, J.-M. *Nature* **2008**, *451*, 652−657.
(2) Zhang, W.-J. J. *Power Sources* **2011**, *196*, 13−24.
(3) Chan, C. K.; Peng, H.; Liu, G.; McIlwrath, K.; Zhang, X. F.; Huggins, R. A.; Cui, Y. High-performance lithium battery anodes using silicon nanowires. *Nat. Nanotechnol.* **2008**, *3*, 31−35.
(4) Chemical element. *Encyclopedia Britannica Online* 2012; http://www.britannica.com/EBchecked/topic/108636/chemical-element, accessed April 17, 2012.
(5) Xu, K. *Chem. Rev.* **2004**, *104*, 4303−4417.

(6) Xu, K.; Von Cresce, A. *J. Mater. Chem.* **2011**, *21*, 9849−9864.
(7) Aurbach, D. J. *Power Sources* **2000**, *89*, 206−218.
(8) Lee, S. W.; McDowell, M. T.; Berla, L. A.; Nix, W. D.; Cui, Y. *Proc. Natl. Acad. Sci. U.S.A.* **2012**, *109*, 4080−4085.
(9) Liu, X. H.; Zhong, L.; Huang, S.; Mao, S. X.; Zhu, T.; Huang, J. Y. *ACS Nano* **2012**, *6*, 1522−1531.
(10) Park, M.-H.; Kim, M. G.; Joo, J.; Kim, K.; Kim, J.; Ahn, S.; Cui, Y.; Cho, J. *Nano Lett.* **2009**, *9*, 3844−3847.
(11) Magasinski, A.; Dixon, P.; Hertzberg, B.; Kvit, A.; Ayala, J.; Yushin, G. *Nat. Mater.* **2010**, *9*, 353−358.
(12) Song, T.; Xia, J.; Lee, J.-H.; Lee, D. H.; Kwon, M.-S.; Choi, J.-M.; Wu, J.; Doo, S. K.; Chang, H.; Park, W. I.; Zang, D. S.; Kim, H.; Huang, Y.; Hwang, K.-C.; Rogers, J. A.; Paik, U. *Nano Lett.* **2010**, *10*, 1710−1716.
(13) Magasinski, A.; Zdyrko, B.; Kovalenko, I.; Hertzberg, B.; Burtovyy, R.; Huebner, C. F.; Fuller, T. F.; Luzinov, I.; Yushin, G. *ACS Appl. Mater. Interfaces* **2010**, *2*, 3004−3010.
(14) Mazouzi, D.; Lestriez, B.; Roué, L.; Guyomard, D. *Electrochem. Solid-State Lett.* **2009**, *12*, A215−A218.
(15) Liu, G.; Xun, S.; Vukmirovic, N.; Song, X.; Olalde-Velasco, P.; Zheng, H.; Battaglia, V. S.; Wang, L.; Yang, W. *Adv. Mater.* **2011**, *23*, 4679−4683.
(16) Kovalenko, I.; Zdyrko, B.; Magasinski, A.; Hertzberg, B.; Milicev, Z.; Burtovyy, R.; Luzinov, I.; Yushin, G. *Science* **2011**, *75*, 75−79.
(17) Yoshio, M.; Wang, H.; Fukuda, K.; Umeno, T.; Dimov, N.; Ogumi, Z. J. *Electrochem. Soc.* **2002**, *149*, A1598−A1603.
(18) Dimov, N.; Kugino, S.; Yoshio, M. *Electrochim. Acta* **2003**, *48*, 1579−1587.
(19) McDowell, M. T.; Woo Lee, S.; Wang, C.; Cui, Y. *Nano Energy* **2012**, *1*, 401−410.
(20) Wu, H.; Chan, G.; Choi, J. W.; Ryu, I.; Yao, Y.; McDowell, M. T.; Lee, S. W.; Jackson, A.; Yang, Y.; Hu, L.; Cui, Y. *Nat. Nanotechnol.* **2012**, DOI: 10.1038/nnano.2012.35.
(21) Wu, H.; Zheng, G.; Liu, N.; Carney, T. J.; Yang, Y.; Cui, Y. *Nano Lett.* **2012**, *12*, 904−909.
(22) Hwang, T. H.; Lee, Y. M.; Kong, B.-S.; Seo, J.-S.; Choi, J. W. *Nano Lett.* **2012**, *12*, 802−807.
(23) Li, X.; Meduri, P.; Chen, X.; Qi, W.; Engelhard, M. H.; Xu, W.; Ding, F.; Xiao, J.; Wang, W.; Wang, C.; Zhang, J.-guang; Liu, J. *J. Mater. Chem.* **2012**, DOI: 10.1039/C2JM31286G.
(24) Xu, X.; Deng, C.; Gao, M.; Yu, W.; Yang, P.; Zhang, X. *Adv. Mater.* **2006**, *18*, 3289−3293.
(25) Stober, W. J. *Colloid Interface Sci.* **1968**, *26*, 62−69.
(26) Deng, Y.; Qi, D.; Deng, C.; Zhang, X.; Zhao, D. J. *Am. Chem. Soc.* **2008**, *130*, 28−29.
(27) Beaulieu, L. Y.; Eberman, K. W.; Turner, R. L.; Krause, L. J.; Dahn, J. R. *Electrochem. Solid-State Lett.* **2001**, *4*, A137−A140.
(28) Lee, H.; Dellatore, S. M.; Miller, W. M.; Messersmith, P. B. *Science* **2007**, *318*, 426−430.
(29) Flörke, O. W.; Graetsch, H. A.; Brunk, F.; Benda, L.; Paschen, S.; Bergna, H. E.; Roberts, W. O.; Welsh, W. A.; Libanati, C.; Ettlinger, M.; Kerner, D.; Maier, M.; Meon, W.; Schmoll, R.; Gies, H.; Schiffmann, D. In *Ullmann's Encyclopedia of Industrial Chemistry*; Wiley-VCH Verlag GmbH & Co.: Weinheim, Germany, 2000.
(30) Liu, R.; Mahurin, S. M.; Li, C.; Unocic, R. R.; Idrobo, J. C.; Gao, H.; Pennycook, S. J.; Dai, S. *Angew. Chem., Int. Ed.* **2011**, *50*, 6799−6802.
(31) Zhao, L.; Hu, Y.-S.; Li, H.; Wang, Z.; Chen, L. *Adv. Mater.* **2011**, *23*, 1385−1388.
(32) Huang, J. Y.; Zhong, L.; Wang, C. M.; Sullivan, J. P.; Xu, W.; Zhang, L. Q.; Mao, S. X.; Hudak, N. S.; Liu, X. H.; Subramanian, A.; Fan, H.; Qi, L.; Kushima, A.; Li, J. *Science* **2010**, *330*, 1515−1520.
(33) Wang, C.-M.; Li, X.; Wang, Z.; Xu, W.; Liu, J.; Gao, F.; Kovarik, L.; Zhang, J.-G.; Howe, J.; Burton, D. J.; Liu, Z.; Xiao, X.; Thevuthasan, S.; Baer, D. R. *Nano Lett.* **2012**, *12*, 1624−1632.
(34) Limthongkul, P.; Jang, Y.-I.; Dudney, N. J.; Chiang, Y.-M. *Acta Mater.* **2003**, *51*, 1103−1113.
(35) Chon, M. J.; Sethuraman, V. A.; McCormick, A.; Srinivasan, V.; Guduru, P. R. *Phys. Rev. Lett.* **2011**, *107*, 045503.
(36) Iwamura, S.; Nishihara, H.; Kyotani, T. *J. Phys. Chem. C* **2012**, *116*, 6004−6011.
(37) McDowell, M. T.; Lee, S. W.; Ryu, I.; Wu, H.; Nix, W. D.; Choi, J. W.; Cui, Y. *Nano Lett.* **2011**, *11*, 4018−4025.
(38) Xun, S.; Song, X.; Wang, L.; Grass, M. E.; Liu, Z.; Battaglia, V. S.; Liu, G. J. *Electrochem. Soc.* **2011**, *158*, A1260−A1266.
(39) Liu, N.; Hu, L.; McDowell, M. T.; Jackson, A.; Cui, Y. *ACS Nano* **2011**, *5*, 6487−6493.